signals

MDPI

Article

Noncooperative Spectrum Sensing Strategy Based on Recurrence Quantification Analysis in the Context of the Cognitive Radio

Jean-Marie Kadjo [1,2], Koffi Clément Yao [1], Ali Mansour [2,*] and Denis Le Jeune [2]

[1] LABSTICC UMR CNRS 6285, Université de Bretagne Occidentale, 29238 Brest, France; jmn.kadjo@gmail.com (J.-M.K.); koffi-clement.yao@univ-brest.fr (K.C.Y.)
[2] Lab-STICC, UMR 6285, ENSTA Bretagne, 29806 Brest, France; dlejeune29@sfr.fr
* Correspondence: mansour@ieee.org

Abstract: This paper addresses the problem of noncooperative spectrum sensing in very low signal-to-noise ratio (SNR) conditions. In our approach, detecting an unoccupied bandwidth consists of detecting the presence or absence of a communication signal on this bandwidth. Digital communication signals may contain hidden periodicities, so we use Recurrence Quantification Analysis (RQA) to reveal the hidden periodicities. RQA is very sensitive and offers reliable estimation of the phase space dimension m or the time delay τ. In view of the limitations of the algorithms proposed in the literature, we have proposed a new algorithm to simultaneously estimate the optimal values of m and τ. The new proposed optimal values allow the state reconstruction of the observed signal and then the estimation of the distance matrix. This distance matrix has particular properties that we have exploited to propose a Recurrence-Analysis-based Detector (RAD). The RAD can detect a communication signal in a very low SNR condition. Using Receiver Operating Characteristic curves, our experimental results corroborate the robustness of our proposed algorithm compared with classic widely used algorithms.

Keywords: cognitive radio; dynamic spectrum access; spectrum sensing; embedding parameters; false nearest neighbors; recurrence quantification analysis

Citation: Kadjo, J.-M.; Yao, K.C.; Mansour, A.; Le Jeune, D. Noncooperative Spectrum Sensing Strategy Based on Recurrence Quantification Analysis in the Context of the Cognitive Radio. *Signals* **2024**, *5*, 438–459. https://doi.org/10.3390/signals5030022

Academic Editors: Santiago Marco and Chenglong Shao

Received: 24 July 2023
Revised: 18 June 2024
Accepted: 25 June 2024
Published: 1 July 2024

1. Introduction

The need to make better use of the radio spectrum is leading to the development of new spectrum access strategies. Among these strategies, the opportunistic spectrum access based on the cognitive radio concepts allows the sharing of a spectral bandwidth between two categories of users: Primary User "PU" and Secondary User "SU". The PU holds the license to exploit the bandwidth, and the SU is an opportunistic user willing to use the channel when the PU is idle. One of the most crucial challenges for the SU is the identification of a free bandwidth by conducting a spectrum sensing [1,2]. Many reliable spectrum sensing methods have been developed to help the SU limit their interference to the PU's transmission [3–11]. Among the spectrum sensing approaches, we can mention Waveform Detection (WFD) [12], Cyclostationary-Features-based Detection (CFD) [13], and Energy-based Detection (ED) [14,15]. One of the most reliable methods, WFD, requires prior knowledge of the PU's signal characteristics. Based on the cyclic spectrum estimation, the CFD requires a relatively high computational cost for a high-frequency resolution. ED is the simplest detection method, but it is unable to distinguish a communication signal from an energetic noise when the noise is not a weak-sense stationary stochastic process or the signal-to-noise ratio (SNR) is very low. Recently, spectrum sensing algorithms, based on the promising concept of machine or deep learning, have been proposed [16–19]. However, these algorithms do not perform well in a noncooperative context or at a low SNR (SNR ≤ -3 dB) and require a huge database to be optimized. To overcome these issues, we developed a blind strategy based on the Recurrence Quantification Analysis

(RQA) of the received signal [20]. RQA is a nonlinear data analysis technique applied to various fields to study the dynamics of complex systems. It is particularly useful for analyzing time series data that exhibit nonlinear, nonstationary, or chaotic behavior. It is widely introduced in the financial sector, particularly in the analysis of cryptocurrencies like Bitcoin [21]. In the field of cardiology, RQA has been also employed to understand the nonlinear dynamics of heart rate variability after acutely induced myocardial ischemia by percutaneous transluminal coronary angioplasty [22]. RQA is a versatile tool that has been applied to a wide range of applications, from financial markets and cardiology to atmospheric science, urban management, and neurocognitive research. Its ability to reveal important properties of time series data, such as determinism, laminarity, stability, randomness, regularity, and complexity, makes it a valuable technique for analyzing the dynamics of complex systems across various domains [21–25]. In this paper, we propose to use RQA in digital communications, because it is able to reveal some intrinsic features of digital communication signals, such as hidden periodicities, stationarity features, or linearity properties. Indeed, due to modulation standards, transmitted signals may contain hidden periodicities. Using this fact, we use Recurrence Quantification Analysis (RQA) tools to detect if the bandwidth allocated to the PU is available or not. The main RQA tool used to quantify the recurrence level is the Recurrence Rate (RR), which is considered the probability of having recurring states in a signal. In a recent work, we proposed an RR-based Detector (RRD) [20]. However, the RRD is very sensitive to SNRs and depends on the choice of a recurrence threshold. To overcome the RRD's limits, in this paper, we propose an efficient algorithm called the Recurrence-Analysis-based Detector (RAD). The RAD exploits the similitude of distances among various states of the signal in a multidimensional space. This similitude of distances is evaluated by a square symmetrical matrix named the distance matrix. Using symmetrical properties, we only exploit the upper triangular part of this matrix in order to considerably reduce the computational cost of the RAD. Then, we show that for a White Gaussian Noise (WGN), the coefficients of the first top diagonal of the distance matrix become a representative sample of all other coefficients. This is not the case for a communication signal even with a small SNR. This new approach can detect a communication signal in a very low SNR. We have analytically established the probabilities of detection P_d and false alarm P_{fa}. Through Monte Carlo simulations, we studied the Receiver Operating Characteristic (ROC) curves of the RAD. The theoretical and experimental results show the ability of the RAD to detect the presence of a communication signal as soon as the SNR is greater than -12 dB with a very low probability of a false alarm.

The rest of this paper is organized as follows: Section 2 presents the problem of spectrum sensing and our motivation for RQA. Section 3 deals with the concepts of RQA and the state of the art in the determination of embedding parameters in order to exhibit the hidden recurrences. Sections 4 and 5 present the Recurrence-Analysis-based detector model and its theoretical and experimental performance. The last section contains the conclusion and perspectives.

2. Spectrum Sensing Problem

The radio spectrum is a limited natural resource. Many techniques, such as cooperative communication systems and heterogeneous networks, have been developed to deal with this scarcity of the radio spectrum [26]. However, none of them can meet the strong demand for radio spectrum. The cognitive radio introduced by Mitola [27,28] is a promising solution allowing dynamic access to the radio spectrum [1]. Dynamic spectrum access (DSA) is defined as a technique by which the operating spectrum of a radio network can be selected dynamically from the available spectrum [26]. The DSA allows the SU to exploit the holes in the spectrum dedicated to the PU. The great challenge of DSA for the SU remains the spectrum sensing stage, during which the SU should detect the presence of the PU on a given bandwidth.

2.1. Spectrum Sensing as a Statistical Decision

The PU's signal detection by the SU can be modeled as a binary hypothesis testing problem, given as [26]:

- Hypothesis $\mathcal{H}_0$: PU's signal is absent
- Hypothesis $\mathcal{H}_1$: PU's signal is present

Let $y(n)$ be the signal observed by the Secondary User (SU):

$$y(n) = hs(n) + b(n) \tag{1}$$

where h is the channel gain and $b(n)$ is the channel noise. The noise samples b_k are assumed to be independent and identically distributed (i.i.d). The noise $b(n)$ is a Complex Circular Gaussian variable $\left(\mathrm{E}[b(n)] = 0; \mathrm{E}\left[|b(n)|^2\right] = \sigma_b^2\right)$; E[.] denotes the mathematical expectation.

The Test Statistic T should be compared with a predetermined threshold λ for decision making. In this case, the probability of false alarm P_{fa} and the probability (Pr) of detection P_d [29] are defined as follows:

$$P_{fa} \triangleq Pr\{T \geq \lambda | \mathcal{H}_0\} \tag{2}$$

$$P_d \triangleq Pr\{T > \lambda | \mathcal{H}_1\} \tag{3}$$

where $\triangleq$ stands for equal by definition.

For good performance, P_d should be increased as much as possible while keeping P_{fa} under a small preselected value. In the noncooperative spectrum sensing context, the detection algorithms should be able to find out intrinsic features of the communication signal to enhance a spectrum sensing task. One of the main features can be the recurrence of internal states in the communication signals. Hereinafter, we develop a robust algorithm based on RQA.

2.2. RQA Benefits

The RQA enjoys several specific properties:

1. RQA is based on the chaos theory and is normally used to extract the hidden recurring states of a dynamic system. The various parts of a transmission chain, such as modulation, filtering, coding, multiplexing, etc, generate hidden recurring states in the communication signals. Therefore, RQA can help detect the presence of the PU's signal on a desired bandwidth.
2. In a previous work [20], we showed that RQA is a promising tool for the spectrum sensing task. Indeed, in a noncooperative context, we proposed the Recurrence-Rate-based detection model (RRD), and this previous algorithm was able to detect the presence of the PU's signals with SNR ≥ -5 dB.
3. During the detection procedure, a spectrum sensing algorithm based on RQA does not require the estimation of the noise variance, as required by some spectrum sensing algorithms such as ED, which is a great advantage.
4. RQA can help detect a communication signal in a very low SNR; and contrary to ED, Recurrence Analysis can distinguish a noisy communication signal from a high energy noise.
5. RQA does not have a high computational cost like CFD. In noncooperative spectrum sensing, RQA is more robust compared with the widely used ED or CFD.

3. Recurrence Quantification Analysis

Recurrence is a fundamental feature of dynamic systems that can be exploited to study the behavior of these systems and to discover their intrinsic properties [20,30,31]. To analyze hidden recurrences in dynamic and nonlinear systems, an important concept in the chaos theory, in which RQA can be used [32–35]. During the evolution of a dynamic system, some internal states can be quasi-periodically repeated. In the phase space, the successive states of a dynamic system form trajectories that characterize the temporal evolution of the

system. Knowing the temporal evolution equation, any state of the system can be precisely determined at any time. Unfortunately in real-world situations, this equation is unknown; instead, we dispose only of a sequence of scalar measurements as time series [36,37]. From these time series, we should reconstruct the phase space. The gold standard method for the phase space reconstruction is delay-coordinate embedding [36]. The objective of a delay-coordinate embedding method is to use the delayed versions of $y(n)$ to form a multidimensional observable $\mathbf{x}_k$ called state vector or state of $y(n)$. The state vector $\mathbf{x}_k$ at moment k is defined as follows:

$$\mathbf{x}_k = [y_k, y_{k+\tau}, \cdots, y_{k+(m-1)\tau}]^T \tag{4}$$

where y_k denotes the sample of y at the moment k, τ is the time delay, and m is the embedding dimension. The main challenge for the delay-coordinate embedding method is the reliable estimation of τ and m.

3.1. Estimation of the Embedding Parameters

3.1.1. Time Delay

Theoretically, the time delay τ can be almost arbitrarily chosen if the observation $y(n)$ is noise-free with an infinite number of samples. However, these conditions cannot be satisfied in real applications because of noise which can generate statistical dependence among the state vectors $\mathbf{x}_k$. Therefore, the time delay τ has to be wisely chosen in order to reduce this statistical dependence [20,36,38]. To determine the optimal time delay τ_0, one can use the autocorrelation function, Average Mutual Information (AMI), or phase portrait approach. The most appropriate method is the AMI because it measures the general dependence between two random variables [39]. Therefore, it could provide a better criterion for the optimal time delay τ_0. The concept of AMI consists, first of all, in estimating the mutual information $I(\tau)$ between $y(n)$ and its delay version $y(n-\tau)$ by varying the value of τ from 0 to N; N denotes the number of samples contained in $y(n)$. After that, the optimal τ_0 is chosen as the first τ value that minimizes $I(\tau)$ [20,40,41]. Based on Equation (1), we can conclude that $I(\tau)$, and indirectly τ_0, depends on three parameters: the SNR value, the sampling rate, and the modulation scheme. Consequently, using the AMI method to determine τ_0 is not so suitable in the context of a noncooperative spectrum sensing algorithm.

3.1.2. Phase Space Dimension

The optimal embedding dimension m_0 for an observed signal $y(n)$ is the minimum dimension for the state vectors $\mathbf{x}_k$ to give a reliable reconstruction of $y(n)$ phase space [35,37]. From the literature, many approaches to estimate m_0 have been developed [38,42,43]. The most used approach is based on the False Nearest Neighbors (FNNs) method [43]. According to the principle of FNNs, any two true neighboring points in the $m-dimensional$ reconstructed phase space must remain neighbors in the $(m+1)-dimensional$ reconstructed phase space. Otherwise, they are called false neighbors. A perfect embedding means all neighboring points should be true neighbors [20,42,43]. Inspired by the FNN-based algorithm proposed in [42], we identify m_0 by using the distance ratio, $a(i,m)$, defined as follows [42]:

$$a(k,m) = \frac{\left\| \mathbf{x}_k^{(m+1)} - \mathbf{x}_l^{(m+1)} \right\|_\infty}{\left\| \mathbf{x}_k^{(m)} - \mathbf{x}_l^{(m)} \right\|_\infty}; \tag{5}$$

where $k, l =\in \{1, 2, \cdots, N - m\tau\}$; $\mathbf{x}_k^{(m)}$ are the state vectors from the $m-dimensional$ phase space; and $\|.\|_\infty$ is $L-infinity$ norm. The major drawback of using the distance

ratio $a(k,m)$ is its sensitivity to the reference state vector $\mathbf{x}_k$. To overcome this drawback, we consider the average value $\bar{a}(m,\tau)$ instead of $a(k,m)$:

$$\bar{a}(m,\tau) = \frac{1}{N-m\tau} \sum_{k=1}^{N-m\tau} a(k,m) \tag{6}$$

To investigate the dependence of $\bar{a}(m,\tau)$ on m, the coefficient of proximity $r(m,\tau)$ is defined as follows:

$$r(m,\tau) \triangleq \frac{\bar{a}(m+1,\tau)}{\bar{a}(m,\tau)} \tag{7}$$

When m becomes greater than a limit value m_{lim}, the proximity coefficient $r(m,\tau)$ converges to one. Hence, $m_0 = m_{\text{lim}} + 1$ becomes the minimum embedding dimension [42]. Based on Equation (7), we can observe that $r(m,\tau)$ depends on the time delay value τ. This assertion is corroborated by simulation results. Figure 1 illustrates, for example, the evolution of $r(m,\tau)$ for two extreme values of τ; for $\tau = 2$, the optimal value of $m_0 = 6$; whereas for $\tau = 100$, we obtain $m_0 = 9$. As m depends on the choice of τ, we propose hereinafter an optimization strategy to find simultaneously the optimal values of m and τ.

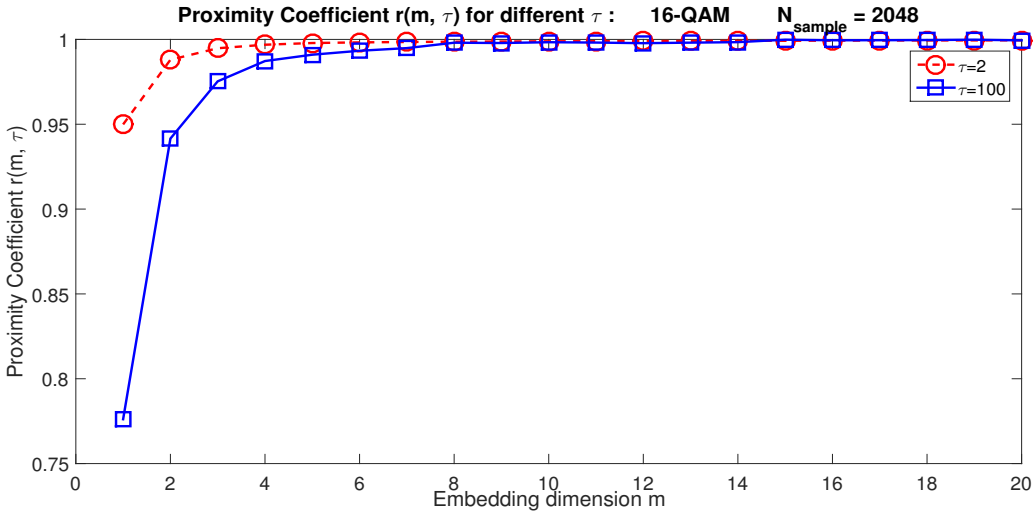

Figure 1. The proximity coefficient $r(m,\tau)$ based on the embedding dimension m for a 16-QAM signal.

3.1.3. Optimal Values of m and τ

$r(m,\tau)$ is a bivariate function whose expression leads to

$$\lim_{(m,\tau)\to(m_0,\tau_0)} r(m,\tau) = 1 \tag{8}$$

So we define the cost function $f(m,\tau)$:

$$f(m,\tau) = \bar{a}(m,\tau) - \bar{a}(m+1,\tau) \tag{9}$$

The optimal values m_0 and τ_0 become

$$(m_0,\tau_0) = \underset{(m,\tau)\in\mathbb{N}^*}{argmin}\{f(m,\tau)\} \tag{10}$$

Numerical results show that values of (m_0,τ_0) obtained from (10) become independent from modulation schemes, SNR, and the number of samples per symbol N_s. Figure 2

illustrates the cost function $\mathbf{f}(m,\tau)$ with respect to (m,τ) for a noisy 16-QAM signal. We can notice that

$$\forall\ \tau \geq 6, \quad m \geq 1, \quad \mathbf{f}(m,\tau) \to 0 \tag{11}$$

The number K of state vectors is given by

$$K = N - (m-1)\tau \geq K_{min} \tag{12}$$

Based on Takens' theorem (in Taken's theorem, the phase space of a system can be reliably reconstructed if and only if $m \geq 2D+1$, where $D \geq 1$ is the dimension of the system attractor [36,44]) and the minimum number K_{min} of state vectors for reliable detection, we conclude that m_0 and τ_0 should be chosen in the following ranges:

$$(m_0,\tau_0) \in \left[\,3\,;\ \frac{N-K_{min}}{\tau_0}\,\right] \times \left[\,6\,;\ \frac{N-K_{min}}{2}\,\right] \tag{13}$$

However, we notice that in practice $K_{min} \ll N$. Consequently, we can

$$(m_0,\tau_0) \in \left[\,3\,;\ \frac{N}{\tau_0}\,\right] \times \left[\,6\,;\ \frac{N}{2}\,\right] \tag{14}$$

The recurring states in the phase space can be highlighted by the Recurrence Plot.

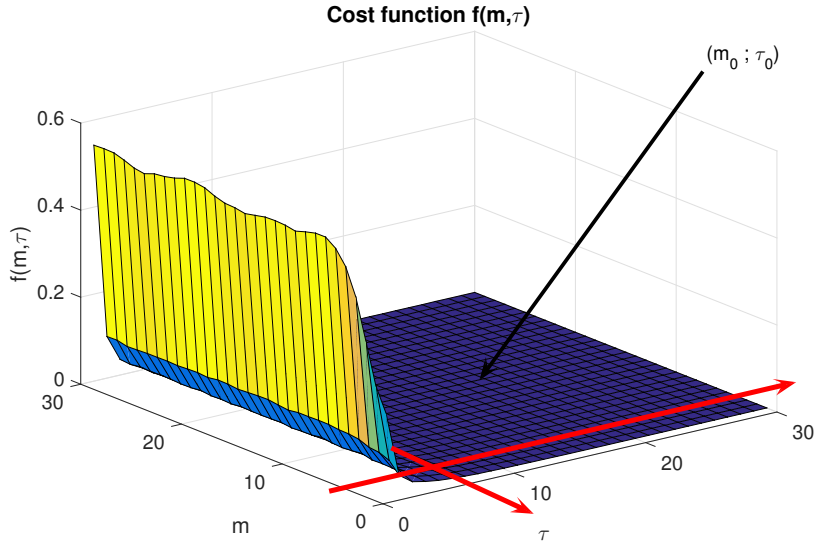

Figure 2. The cost function $\mathbf{f}(m,\tau)$ based on (m,τ): The flat area of the curve $\mathbf{f}(m,\tau)$ corresponds to a set of optimal values of (m,τ). Consequently, the optimal values (m_0,τ_0) of (m,τ) should be chosen as follows $(m_0,\tau_0) \subset \left[\,3\,;\ \frac{N}{\tau_0}\,\right] \times \left[\,6\,;\ \frac{N}{2}\,\right]$.

3.2. Recurrence Plot

The Recurrence Plot (RP) illustrates recurrences contained in a signal. The RP is based on the recurrence matrix $\mathbf{R}_{i,j}^{(\varepsilon,m)}$ [30,36]:

$$\mathbf{R}_{i,j}^{(\varepsilon,m)} = \Theta\Big\{\varepsilon - \big\|\mathbf{x}_i - \mathbf{x}_j\big\|_2\Big\} \tag{15}$$

where $i,j \in \{1,\cdots,K\}$ and $K = N-(m-1)\tau$ denotes the number of reconstructed state vectors $\mathbf{x}_k$; ε is the recurrence threshold, $\Theta(.)$ represents Heavisides' step function, and $\|.\|_2$ is the L_2 or Frobenius norm. $d_{ij} = \big\|\mathbf{x}_i - \mathbf{x}_j\big\|_2$ are the coefficients of the distance matrix M. According to Equation (15), the states $\mathbf{x}_i$ and $\mathbf{x}_j$ are recurring states if $\big\|\mathbf{x}_i - \mathbf{x}_j\big\| < \varepsilon$. In the RP, a recurrence is represented by a black dot. If the parameters m, τ, and ε are optimal,

the RP presents some intrinsic patterns of the system. For example, Figures 3–5 represent, respectively, the RP of 16-QAM signal, GMSK signal, and a random zero mean White Gaussian Noise (WGN) with a variance σ_b^2. We can notice that the patterns in the RP of the 16-QAM signal are different from those of the GMSK signal, whereas the RP of the WGN has no particular pattern. Heuristically, we can set the recurrence threshold as $\varepsilon = 0.5\sigma_y$ where σ_y^2 denotes the variance of the observed signal $y(n)$; the embedding parameters are established as $m = 16$ and $\tau = 6$.

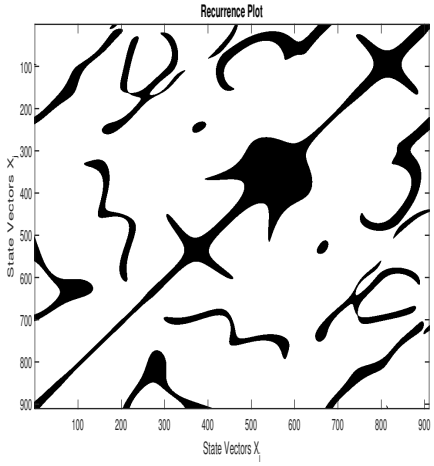

Figure 3. RP according to Equation (15) of a 16-QAM signal.

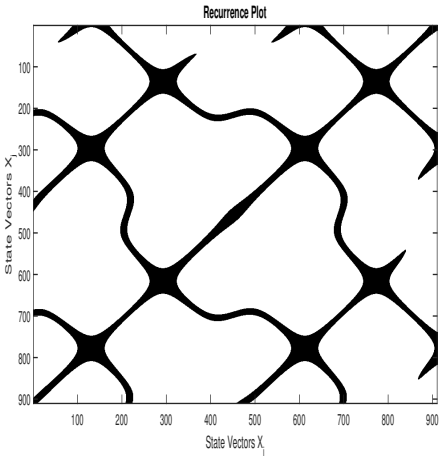

Figure 4. RP of a Gaussian Minimum Shift Keying (GMSK) signal.

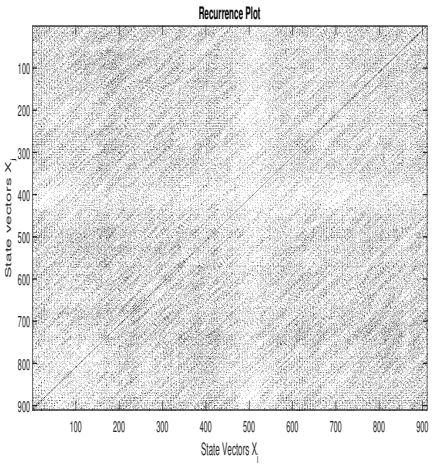

Figure 5. RP of White Gaussian Noise.

As the visual analysis of RP is not objective, Zbilut and Webber introduced a procedure to quantify RP structures [45,46]. In the literature, one has five classical tools to perform the RQA. Some RQA tools are based on the recurrence density, while others use the line structures of the RP [36]. The classical RQA tools are developed and extended in [30,36]. The main challenge with classical or extended RQA tools is the choice of an optimal recurrence threshold ε of Equation (15). A small value of ε does not reveal noticeable occurrences, while a large value of ε may lead to the appearance of neighbors for most of the existing points and cause false occurrences [30,47]. The choice of ε is a delicate issue affecting the reliability of the spectrum sensing based on classical or extended RQA tools [20]. To overcome this issue, we propose in the following sections a new algorithm called the Recurrence-Analysis-based Detector (RAD), which only exploits the distance matrix. This distance matrix does not depend on the recurrence threshold ε and nor does the proposed detection model RAD.

4. Recurrence-Analysis-Based Detector

The Recurrence Rate (RR) is an essential tool of RQA. Our previous works based on the RQA detection model [20] show that an RR-based detection model (RRD) suffers from major shortcomings, as follows:

1. It cannot detect the presence of a communication signal when SNR ≤ -5 dB.
2. It is very sensitive to the recurrence threshold ε.
3. The computational cost is relatively high
4. The performance of an RRD is sensitive to the types of modulations of a communication signal.

To overcome the above limitations, we develop hereinafter a new detection model, the Recurrence Analysis Detection model (RAD), which is able to operate in very low SNR conditions. In order to reduce drastically the computational cost and avoid the delicate issue of the recurrence threshold ε, the RAD only uses the distances $d_{ij} = \left\|\mathbf{x}_i - \mathbf{x}_j\right\|_2$ of the upper triangular part of the distance matrix.

4.1. Detection Model

Usually, the RQA is performed on the entire distance matrix $D = (d_{ij})_{1\leq i,j\leq K}$ of different state vectors. As D is a symmetrical matrix, in order to reduce the computational cost, we use the upper triangular part of D, without the main diagonal defined by its general coefficients:

$$D_{ij} = d_{ij}\,; \quad \forall\, 1 \leq i < j \leq K \tag{16}$$

We denote by $\mathbf{u}_d$ the coefficients of the first upper diagonal of D and by $\mathbf{u}_\Delta$ the other coefficients of the upper triangular part of D, without the main diagonal. $\mathbf{u}_d$ and $\mathbf{u}_\Delta$ verify two great properties:

1. For a WGN, $\mathbf{u}_d$ and $\mathbf{u}_\Delta$ have the same Probability Density Function (PDF), which is not the case for a noisy communication signal. Hence, to detect the presence of a communication signal, we check if $\mathbf{u}_d$ is representative of $\mathbf{u}_\Delta$. For this purpose, we use a statistical test of conformity to evaluate this representativeness [48].
2. The $\mathbf{u}_d$ of a WGN or a communication signal has the same PDF. This remark allows us to design a detector free of noise variance estimation.

To provide a better understanding of this notion of representativeness, we present the histogram of the $\mathbf{u}_d$ and $\mathbf{u}_\Delta$ of WGN and the communication signal, respectively, in Figures 6 and 7, and we define the confidence interval Φ_Δ as follows:

$$\Phi_\Delta = [\overline{\mathbf{u}}_\Delta - \lambda; \overline{\mathbf{u}}_\Delta + \lambda] \tag{17}$$

where $\overline{\mathbf{u}}_\Delta$ is the average value of $\mathbf{u}_\Delta$ and λ is the predetermined detection threshold for RAD. Further details about λ can be found in Section 4.2.4.

On the basis of the histogram of distance and by using Kolmogorov–Smirnov test [49], for a WGN only, we note that $\mathbf{u}_d$ and $\mathbf{u}_\Delta$ can be approximated by the same PDF (see Figure 6). Consequently, by using the statistical test of conformity based on the estimation average value, we show that $\mathbf{u}_d$ is representative of $\mathbf{u}_\Delta$. Indeed, $\overline{\mathbf{u}}_d \in \Phi_\Delta$; $\overline{\mathbf{u}}_d$ denotes the average value of $\mathbf{u}_d$. Contrariwise, Figure 7 gives the histogram of distance for a communication signal buried in the WGN with an SNR= 0 dB; we can notice that $\overline{\mathbf{u}}_d \notin \Phi_\Delta$, so $\mathbf{u}_d$ is not representative of $\mathbf{u}_\Delta$.

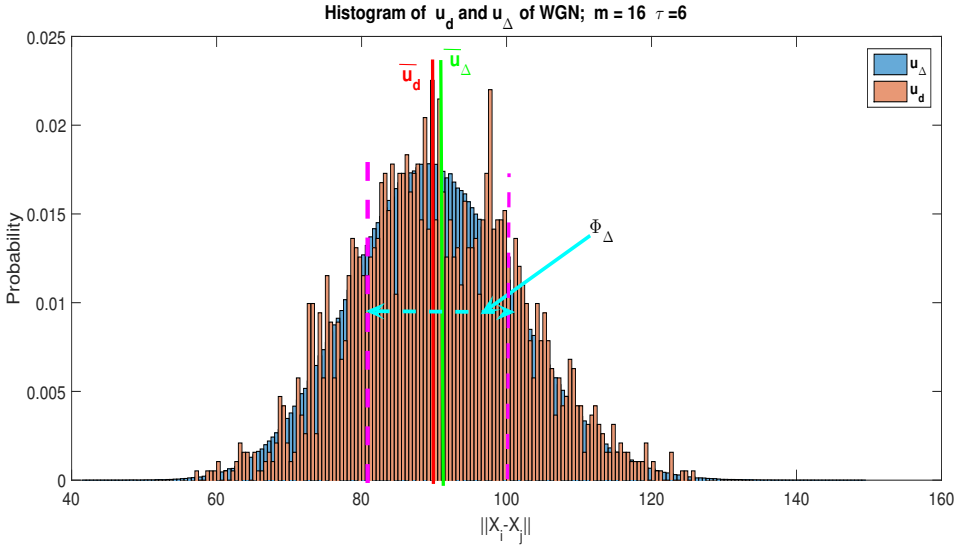

Figure 6. Histogram of $\mathbf{u}_d$ and $\mathbf{u}_\Delta$ for a White Gaussian Noise (WGN): We have $\overline{u}_d = 90.6$ and $\overline{u}_\Delta = 90$. For $P_{fa} = 0.01$, the detection threshold of the RAD becomes $\lambda = 12.5$. Based on the $\overline{u}_\Delta$ value, the confidence interval becomes $\Phi_\Delta = [77.5; 102.5]$. We notice that $\overline{u}_d \in \Phi_\Delta$. Consequently, using the conformity test, we can conclude that $\mathbf{u}_d$ is representative of $\mathbf{u}_\Delta$.

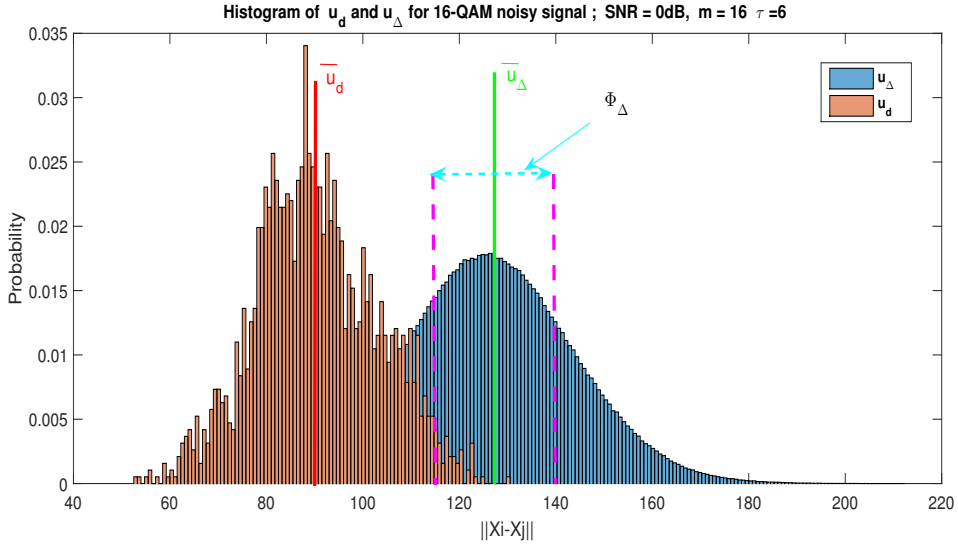

Figure 7. Histogram of $\mathbf{u}_d$ and $\mathbf{u}_\Delta$ for a noisy 16-QAM signal; SNR = 0 dB. In this example, we have $\overline{u}_d = 90$ and $\overline{u}_\Delta = 127$. With $P_{fa} = 0.01$, we obtain $\lambda = 12.5$ and $\Phi_\Delta = [114.5; 139.5]$. We notice that $\mathbf{u}_d$ is not representative of $\mathbf{u}_\Delta$, because $\overline{u}_d \notin \Phi_\Delta$.

Using the statistical test of conformity, we propose the following test statistic T:

$$T = |\overline{\mathbf{u}}_\Delta - \overline{\mathbf{u}}_d| \underset{\mathcal{H}_0}{\overset{\mathcal{H}_1}{\gtrless}} \lambda \tag{18}$$

In the course of our work, we establish the analytical expressions of the probability of detection P_d and the probability of false alarm P_{fa} in order to compare the theoretical and experimental results.

4.2. Analytical Expression of the Probability of False Alarm

The probability of a false alarm P_{fa} can be expressed from the PDF of T under $\mathcal{H}_0$. In order to find this PDF, one should evaluate the PDF of $\overline{\mathbf{u}}_\Delta$ and $\overline{\mathbf{u}}_d$; see Equation (18).

4.2.1. The PDF of $\overline{\mathbf{u}}_\Delta$ under Hypothesis $\mathcal{H}_0$

Under $\mathcal{H}_0$, the average value $\overline{\mathbf{u}}_\Delta$ of $\mathbf{u}_\Delta$ is defined as follows:

$$\overline{\mathbf{u}}_{\Delta/\mathcal{H}_0} = \frac{1}{K_\Delta}\sum_{k=1}^{K_\Delta} u_{\Delta/\mathcal{H}_0}^{(k)} \tag{19}$$

where $K_\Delta = (K-1)(K/2-1)$ and $u_{\Delta/\mathcal{H}_0}^{(k)} \in \{d_{ij}; 1 \le i \le K-2; i+2 \le j \le K\}$.

Based on the central limit theorem for independent random variables and for a large K, $\overline{\mathbf{u}}_{\Delta/\mathcal{H}_0}$ is asymptotically normally distributed with mean $\overline{\mathbf{u}}_{\Delta/\mathcal{H}_0}$ and variance $\sigma^2_{\Delta/\mathcal{H}_0}$:

$$\overline{\mathbf{u}}_{\Delta/\mathcal{H}_0} \mapsto \mathcal{N}\left(\mu_{\Delta/\mathcal{H}_0}, \sigma^2_{\Delta/\mathcal{H}_0}\right) \tag{20}$$

where

$$\mu_{\Delta/\mathcal{H}_0} = \mathbb{E}\left[\overline{\mathbf{u}}_{\Delta/\mathcal{H}_0}\right] \tag{21}$$

$$\sigma^2_{\Delta} = var\left[\overline{\mathbf{u}}_{\Delta/\mathcal{H}_0}\right] \tag{22}$$

To calculate $\mu_{\Delta/\mathcal{H}_0}$ and $\sigma^2_{\Delta/\mathcal{H}_0}$, we can use the PDF $f_{\mathbf{u}_{\Delta/\mathcal{H}_0}}$ (u) of $\mathbf{u}_{\Delta/\mathcal{H}_0}$. An outcome $u_{\Delta/\mathcal{H}_0}$ of $\mathbf{u}_{\Delta/\mathcal{H}_0}$ is given by

$$u_{\Delta/\mathcal{H}_0} = d_{ij} = \sqrt{\sum_{k=0}^{m-1}\left(b_{i+k\tau} - b_{j+k\tau}\right)^2} \tag{23}$$

As $b(n) \mapsto \mathcal{N}(0, \sigma_b^2)$, then $b_{i+k\tau} - b_{j+k\tau} \mapsto \mathcal{N}(0, 2\sigma_b^2)$ and $v_k = \left(\frac{b_{i+k\tau} - b_{j+k\tau}}{\sigma_b\sqrt{2}}\right) \mapsto \mathcal{N}(0,1)$.

By setting $Z = \sqrt{\sum_{k=0}^{m-1} v_k^2}$, we can conclude that Z follows a Chi distribution $\chi(m)$ with m degrees of freedom [50,51]:

$$Z = \frac{\mathbf{u}_{\Delta/\mathcal{H}_0}}{\sigma_b\sqrt{2}} \mapsto \succ(m) \tag{24}$$

The expectation value $\mathbb{E}[Z]$ and variance $var[Z]$ of Z are given as follows [50,51]:

$$\mathbb{E}[Z] = \mu_Z = \sqrt{2}\frac{\Gamma\left(\frac{m+1}{2}\right)}{\Gamma\left(\frac{m}{2}\right)} \tag{25}$$

$$var[Z] = m - \mu_Z^2 \tag{26}$$

where $\Gamma(m) = \int_0^{+\infty} x^{m-1}e^{-x}dx$ is the Gamma function.

From Equation (24), we show that the PDF $f_{\mathbf{u}_{\Delta/\mathcal{H}_0}}$ of $\mathbf{u}_{\Delta/\mathcal{H}_0}$ is defined as follows: [52]:

$$f_{\mathbf{u}_{\Delta/\mathcal{H}_0}}(u) = \frac{u^{m-1}}{2^{m-1}\sigma_b^m\,\Gamma\left(\frac{m}{2}\right)}\exp\left[-\frac{u^2}{4\sigma_b^2}\right] \tag{27}$$

The mean $\mu_{\Delta/\mathcal{H}_0}$ and variance $\sigma^2_{\Delta/\mathcal{H}_0}$ of $\bar{X}_{\Delta/\mathcal{H}_0}$ can be determined by using Equation (24) as follows:

$$\mu_{\Delta/\mathcal{H}_0} = \sigma_b\sqrt{2}\mathbb{E}[Z] \tag{28}$$

$$\sigma^2_{\Delta/\mathcal{H}_0} = \frac{2\sigma_b^2}{K_\Delta} var[Z] \tag{29}$$

Finally, we have $\overline{\mathbf{u}}_{\Delta/\mathcal{H}_0} \mapsto \mathcal{N}\left(\mu_{\Delta/\mathcal{H}_0}, \sigma^2_{\Delta/\mathcal{H}_0}\right)$ with

$$\mu_{\Delta/\mathcal{H}_0} = 2\sigma_b \frac{\Gamma\left(\frac{m+1}{2}\right)}{\Gamma\left(\frac{m}{2}\right)} \tag{30}$$

$$\sigma^2_{\Delta/\mathcal{H}_0} = \frac{2\sigma_b^2}{K_\Delta}\left[m - 2\left(\frac{\Gamma\left(\frac{m+1}{2}\right)}{\Gamma\left(\frac{m}{2}\right)}\right)^2\right] \tag{31}$$

4.2.2. The PDF of $\overline{\mathbf{u}}_d$ under Hypothesis $\mathcal{H}_0$

Under $\mathcal{H}_0$, the average value $\overline{\mathbf{u}}_d$ of $\mathbf{u}_d$ is defined as follows:

$$\overline{\mathbf{u}}_{d/\mathcal{H}_0} = \frac{1}{K_d}\sum_{k=1}^{K_d} u^{(k)}_{d_k/\mathcal{H}_0} \tag{32}$$

where $u^{(k)}_{d/\mathcal{H}_0} \in \{d_{i,i+1}\}; 1 \leq i \leq K_d = K-1$.

Because of the structure of the upper triangular distance matrix, the coefficients of the first top diagonal $u^{(k)}_{d/\mathcal{H}_0}$ are strongly decorrelated. In addition, K_d is a large number. Thus, we can approximate $\overline{\mathbf{u}}_d$ by a Gaussian variable by using the central limit theorem:

$$\overline{\mathbf{u}}_{d/\mathcal{H}_0} \mapsto \mathcal{N}\left(\mu_{d/\mathcal{H}_0}, \sigma^2_{d/\mathcal{H}_0}\right) \tag{33}$$

Using a similar approach to the calculation of the expectation value $\mu_{\Delta/\mathcal{H}_0}$ and variance $\sigma^2_{\Delta/\mathcal{H}_0}$ of $\overline{\mathbf{u}}_{\Delta/\mathcal{H}_0}$, we obtain

$$\mu_{d/\mathcal{H}_0} = 2\sigma_b \frac{\Gamma\left(\frac{m+1}{2}\right)}{\Gamma\left(\frac{m}{2}\right)} \tag{34}$$

$$\sigma^2_{d/\mathcal{H}_0} = \frac{2\sigma_b^2}{K_d}\left[m - 2\left(\frac{\Gamma\left(\frac{m+1}{2}\right)}{\Gamma\left(\frac{m}{2}\right)}\right)^2\right] \tag{35}$$

4.2.3. The Probability Density Function of T under hypothesis $\mathcal{H}_0$

$\overline{\mathbf{u}}_{d/\mathcal{H}_0}$ and $\overline{\mathbf{u}}_{\Delta/\mathcal{H}_0}$ are Gaussian random variables. Based on Equations (20), (30), (31) and (33)–(35) we end up with

$$\overline{\mathbf{u}}_{\Delta/\mathcal{H}_0} - \overline{\mathbf{u}}_{d/\mathcal{H}_0} \mapsto \mathcal{N}\left(0, \sigma_0^2\right) \tag{36}$$

where

$$\sigma_0^2 = \sigma^2_{\Delta/\mathcal{H}_0} + \sigma^2_{d/\mathcal{H}_0} - 2Cov\left(\overline{\mathbf{u}}_{d/\mathcal{H}_0}, \overline{\mathbf{u}}_{\Delta/\mathcal{H}_0}\right) \tag{37}$$

Applying the random variable transformation theorem [52,53] on T from Equation (18), we end up with $t \geq 0$:

$$f_{T/\mathcal{H}_0}(t) = \frac{2}{\sigma_0\sqrt{2\pi}} \exp\left[-\frac{t^2}{2\sigma_0^2}\right] \tag{38}$$

4.2.4. Probability of False Alarm and Detection Threshold

Based on Equation (38), the P_{fa} is expressed as follows:

$$P_{fa} = \int_{\lambda}^{\infty} f_{T/\mathcal{H}_0}(t)dt = erfc\left(\frac{\lambda}{\sigma_0\sqrt{2}}\right) \tag{39}$$

$erfc(x)$ denotes the Complementary Error Function—the Complementary Error Function $erfc(x)$ is defined as follows:

$$erfc(x) = \frac{2}{\sqrt{\pi}} \int_{x}^{+\infty} e^{-\theta^2} d\theta$$

—and the detection threshold λ is

$$\lambda = \sigma_0\sqrt{2}\, erfc^{-1}\left(P_{fa}\right) \tag{40}$$

4.3. Analytical Expression of the Probability of Detection

Taking into account the presence of the communication signal $s(n)$ and keeping the same approach as under H_0, we demonstrate that

$$\overline{\mathbf{u}}_{\Delta/H_1} \mapsto \mathcal{N}\left(\mu_{\Delta/H_1}, \sigma^2_{\Delta/H_1}\right) \tag{41}$$

$$\overline{\mathbf{u}}_{d/H_1} \mapsto \mathcal{N}\left(\mu_{d/H_1}, \sigma^2_{d/H_1}\right) \tag{42}$$

where

$$\mu_{\Delta/H_1} = 2\sqrt{\sigma_s^2 + \sigma_b^2}\, \frac{\Gamma\left(\frac{m+1}{2}\right)}{\Gamma\left(\frac{m}{2}\right)} \tag{43}$$

$$\sigma^2_{\Delta/H_1} = \frac{2(\sigma_s^2 + \sigma_b^2)}{K_\Delta}\left[m - 2\left(\frac{\Gamma\left(\frac{m+1}{2}\right)}{\Gamma\left(\frac{m}{2}\right)}\right)^2\right] \tag{44}$$

$$\mu_{d/H_1} = 2\sigma_b \frac{\Gamma\left(\frac{m+1}{2}\right)}{\Gamma\left(\frac{m}{2}\right)} \tag{45}$$

$$\sigma^2_{d/H_1} = \frac{2\sigma_b^2}{K_d}\left[m - 2\left(\frac{\Gamma\left(\frac{m+1}{2}\right)}{\Gamma\left(\frac{m}{2}\right)}\right)^2\right] \tag{46}$$

We deduce the PDF of T under the hypothesis H_1 as follows:

$$f_{T/H_1}(t) = \frac{1}{\sigma_1\sqrt{2\pi}}\left[e^{-\left(\frac{t-\mu_1}{\sigma_1\sqrt{2}}\right)^2} + e^{-\left(\frac{t+\mu_1}{\sigma_1\sqrt{2}}\right)^2}\right] \tag{47}$$

with $t \geq 0$. μ_1 and σ_1^2 are given by

$$\mu_1 = \mu_{\Delta/H_1} - \mu_{d/H_1}, \tag{48}$$

$$\sigma_1^2 = \sigma_{\Delta/H_1}^2 + \sigma_{d/H_1}^2 - 2Cov(\overline{\mathbf{u}}_{\Delta/H_1}, \overline{\mathbf{u}}_{d/H_1}) \tag{49}$$

Consequently, the Probability of Detection P_d becomes

$$\begin{aligned} P_d &= \int_{\lambda}^{+\infty} f_{T/H_1}(t)dt \\ &= 1 - \frac{1}{2}\left[erfc\left(\frac{-\lambda-\mu_1}{\sigma_1\sqrt{2}}\right) - erfc\left(\frac{\lambda-\mu_1}{\sigma_1\sqrt{2}}\right)\right] \end{aligned} \tag{50}$$

5. Simulations Results

To evaluate the efficiency and the robustness of the proposed detection method, we generate Receiver Operating Characteristic (ROC) curves using Monte Carlo simulations [54,55]. The parameters defined in Table 1 are used with different kinds of communication signals, such as 64-QAM, 16-QAM, BPSK, and 4-ASK.

Table 1. Simulation parameters.

Entity	Parameters	Value
PU's signal	Sampling frequency F_e	128 kHz
	Symbol rate	16 Bd
	Bandwidth of Interest B	24 kHz
SU's Detector	Observation time	15.6 ms
	Sampling Frequency	128 KHz
Embedding parameters	Dimension m	16
	time delay τ	6
Transmission Channel	Noise Model	AWGN

In order to compare the theoretical and experimental performance of the RAD, we generated P_d versus SNR performance curves. Figure 8 shows these performance curves. The theoretical curves were generated by Equation (50) and the experimental curves according to the Monte Carlo simulations. It can be clearly observed that the theoretical results match the simulated ones. From the theoretical and experimental curves, reliable detection is possible as soon as $SNR \geq -12$ dB with $P_d \geq 0.95$ and $P_{fa} = 0.05$.

The Receiver Operating Characteristic curves for different SNR values can be viewed in Figure 9. Here, the RAD is applied on a 16-QAM signal, and the observation time is 31.25 ms. For SNR $= -14$ dB and $P_{fa} = 0.1$, the RAD detects the presence of a communication signal with $P_d = 0.76$, but for SNR $= -13$ dB, $P_d = 0.9$. The detector proves itself powerful as soon as the SNR ≥ -12 dB, since the detection probability $P_d = 0.95$ with a very low value of $P_{fa} = 0.05$; see Figure 9.

Another advantage of the proposed detector is its robustness against any type of classical modulations, such as QAM, PSK, and ASK; see Figure 10, where the ROC curves for 4-ASK, BPSK, and 64-QAM signal are almost identical.

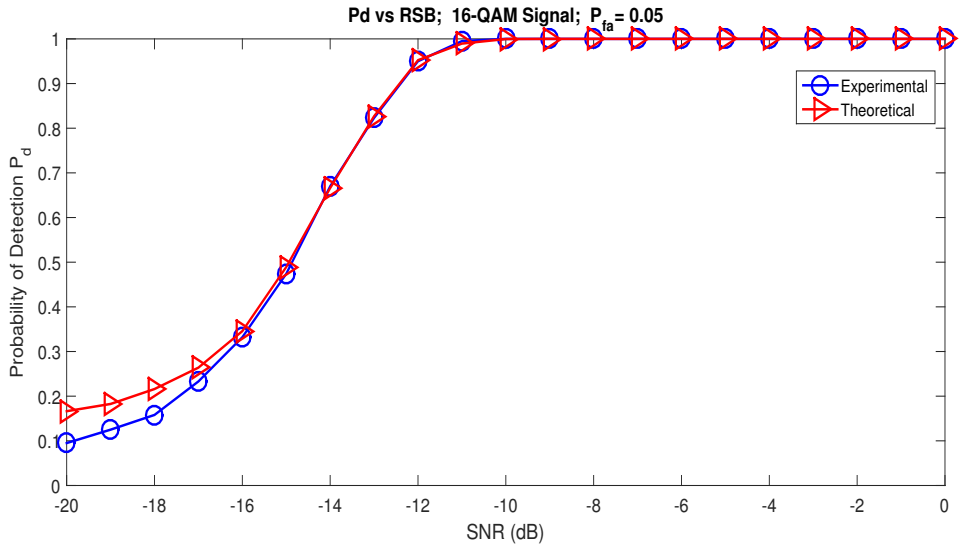

Figure 8. Theoretical and experimental probability of detection for RAD versus SNR.

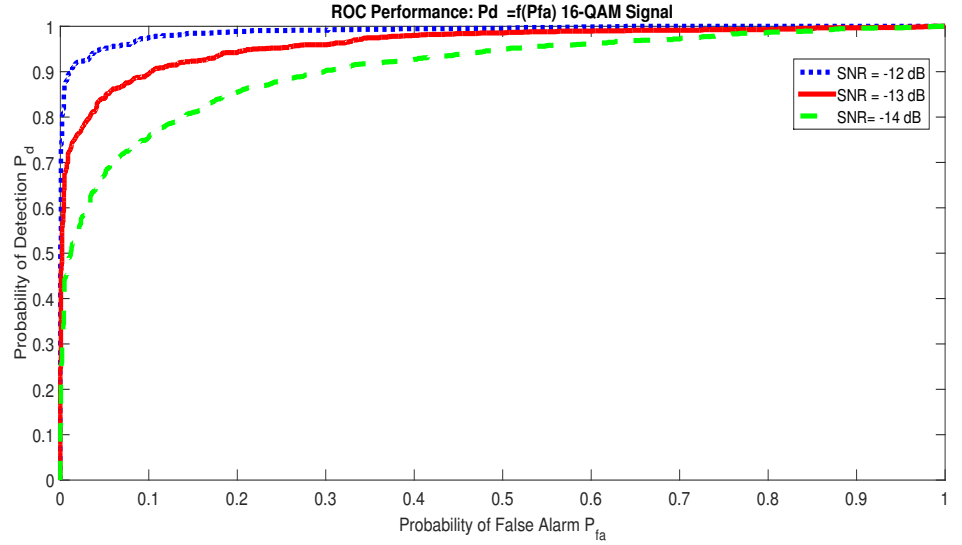

Figure 9. Receiver Operating Characteristic for $16-QAM$ signal.

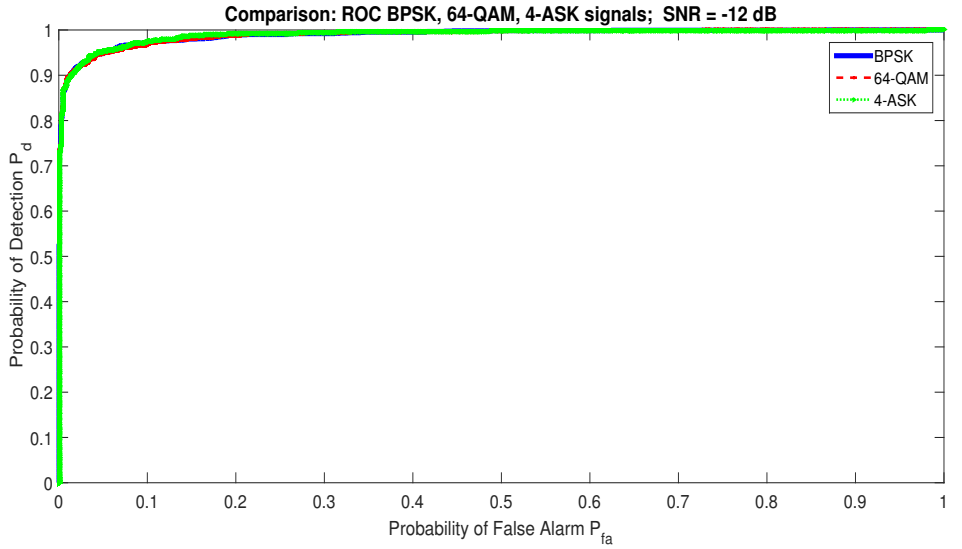

Figure 10. Robust RQA detector insensitivity versus classical modulation techniques.

The performance of RAD increases with the number of samples N. Figure 11 depicts this performance evolution based on N in a Gaussian channel where SNR $=\ -12$ dB. We notice that for $P_{fa} = 0.1$, the RAD detects the communication signal with $P_d = 0.5$ when $N = 500$ samples, with $P_d = 0.8$ when $N = 1000$ samples, and with $P_d = 0.97$ when $N = 2000$ samples.

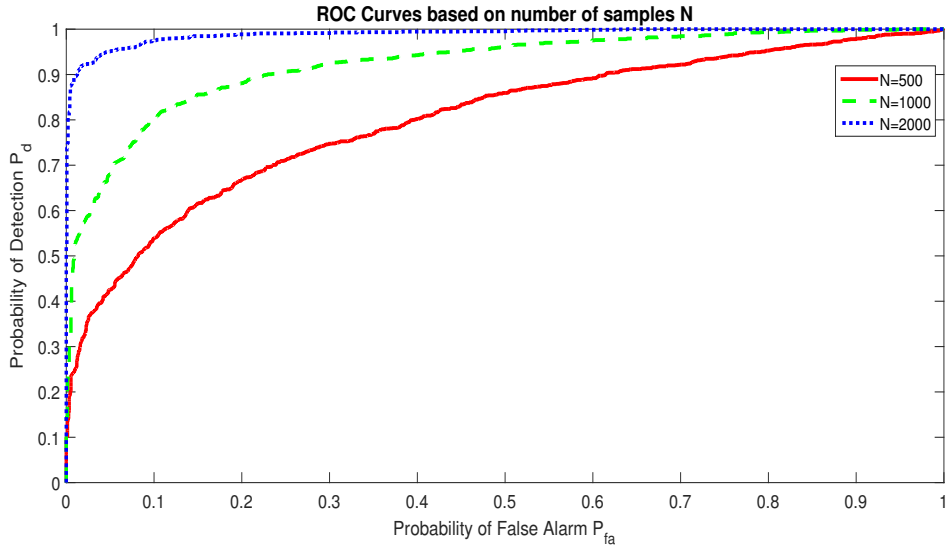

Figure 11. Receiver Operating Characteristic of the RAD model based on the number of observed samples in a Gaussian channel with $SNR = -12$ dB.

By comparing RAD with two other blind spectrum sensing algorithms, Energy Detection (ED) [56] and Cyclostationary Features Detector (CFD) [57,58], and according to the results presented in Figures 12 and 13, we notice the superiority of the RAD to ED and CFD in a Gaussian channel. For example, for the $SNR = -12$ dB and $P_{fa} = 0.05$, the RAD detects the signal with $P_d = 0.95$, whereas the probability of detection for the ED is only $P_d = 0.67$ (see Figure 12). Figure 13 shows that the RAD is able to detect the communication signal in very weak low SNR conditions. For -12 dB $\leqslant$ SNR $\leqslant -10$ dB, the RAD detects the presence of a communication signal with $P_d \geqslant 0.95$ for $P_{fa} = 0.05$. ED achieves RAD performance only when SNR $\geqslant -10$ dB, and CFD works correctly when SNR $\geqslant -7$ dB with $P_d \geqslant 0.97$.

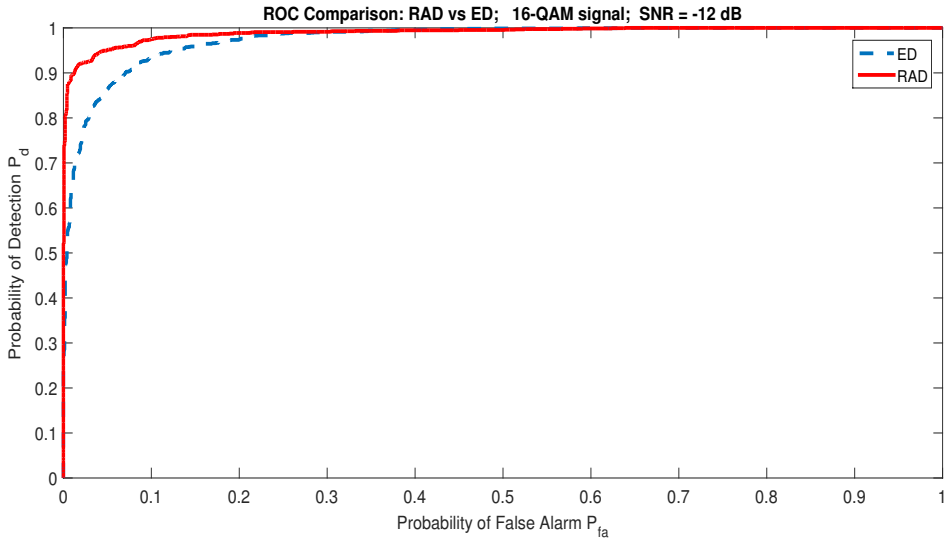

Figure 12. ROC performance: ED vs RAD. The RAD is superior to ED.

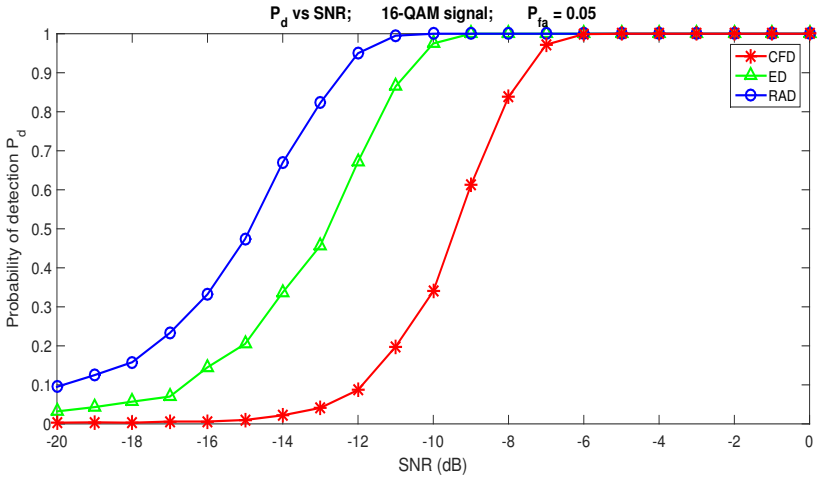

Figure 13. Comparison of Energy Detector (ED), Cyclostationary Features Detector (CFD), and Recurrence Analysis Detector (RAD).

After testing the performance of the detector in a Gaussian channel, we are now interested in the behavior of the RAD in a multipath channel. As a model, we use model D of the Rayleigh channel defined in [59] with the following parameters (Tables 2 and 3):

Table 2. Rayleigh Channel Model Features.

Model D of Rayleigh Channel		
Entity	Parameters	Value
Features	Number of Path	6
	Doppler Frequency $f_{d_{max}}$	1.2 kHz

Table 3. Delay and Gain values for 6 paths [59].

Path Number	1	2	3	4	5	6
Delay (ns)	0	300	8900	12,900	17,100	20,000
Gain (dB)	0	−2.5	−12.8	−10.0	−25.2	−16.0

Figure 14 summarizes the performance of the RAD in a noisy Rayleigh channel. The RAD's performance remains almost unchanged. It detects a communication signal with $P_d \geq 0.92$ with $P_{fa} = 0.05$ as soon as SNR ≥ -12 dB.

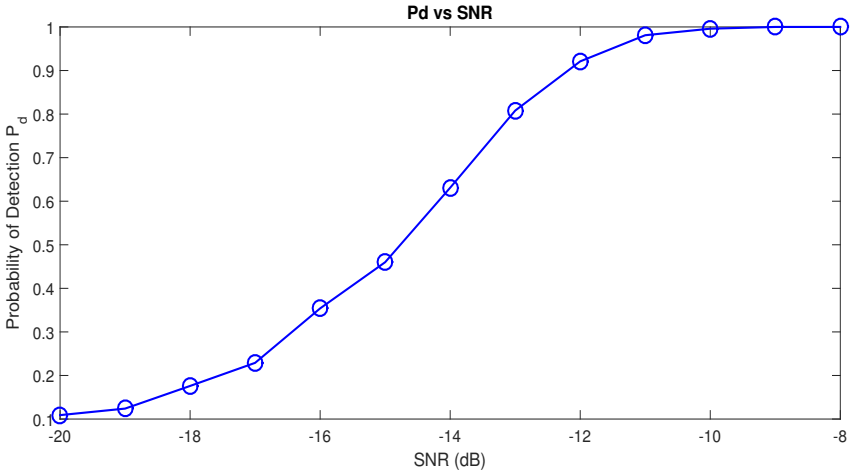

Figure 14. Performance Curve P_d as a function of SNR for 16-QAM signal in a Rayleigh channel.

6. Complexity Analysis of Recurrence-Analysis-Based Detector

Theoretical and experimental analyses show the superiority of the RAD compared with the Energy Detector (ED) and the Cyclostationary Feature Detector (CFD) in a low SNR scenario detection process. The complexity of the algorithms is measured through the number of complex multiplications that the algorithms have to perform for the calculation of the test statistics [60]. In this section, we provide the complexity analyses of the ED, CFD, and RAD.

6.1. Complexity Analysis of Energy-Based Detector

Let $y(n)$ be the observed signal with N samples y_k. The energy $\mathcal{E}_y$ of $y(n)$ is given by

$$\mathcal{E}_y = \frac{1}{N}\sum_{k=1}^{N} y_k^2 \tag{51}$$

The ED detection process is summarized in Figure 15.

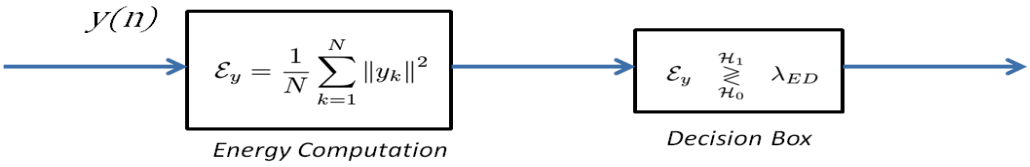

Figure 15. Energy Detector process. λ_{ED} denotes the detection threshold of the ED.

The complexity of the computation can be evaluated according to Equation (51). N multiplication operations are required to perform y_k^2. Consequently, the computation complexity C_{ED} becomes [60]

$$C_{ED} = N \tag{52}$$

6.2. Complexity Analysis of Cyclostationary-Feature-Based Detector

In a blind context, the CFD is based on the reliable estimation of the cyclic spectrum [13,61,62]. The crest factor F_c of the cyclic spectrum can be used as a decision statistic [13]:

$$F_c(\alpha) = \frac{\max_\alpha D(\alpha)}{\sqrt{\frac{1}{2N+1}\sum_{k=1}^{2N+1} D^2(\alpha)}} \underset{\mathcal{H}_0}{\overset{\mathcal{H}_1}{\gtrless}} \lambda_{CFD} \tag{53}$$

where α stands for the cyclic frequency and $D(\alpha)$ denotes the Cyclic Domain Profile (CDP). The computation of F_c requires six steps [13]. First, a Hamming sliding window $w(n)$ is used to apodize the observed signal $y(n)$. Then, we apply a first Fast Fourier Transform (FFT) and calculate the complex demodulates of the apodized signal. After that, we compute the spectral correlation of the different complex demodulates and apply a second FFT. At the end, we obtain the cyclic spectrum, and we compute the crest factor F_c of the cyclic spectrum.

Let N be the number of samples contained in the observed signal $y(n)$ and N_p be the number of samples contained in each apodized block of $y(n)$. $L = \frac{N_p}{4}$ denotes the decimation factor, and $P = \frac{N}{L}$ is the number of apodized blocks from $y(n)$. The apodization is carried out with a Hamming window [13,61,63]. Figure 16 summarizes the essential steps of F_c computation.

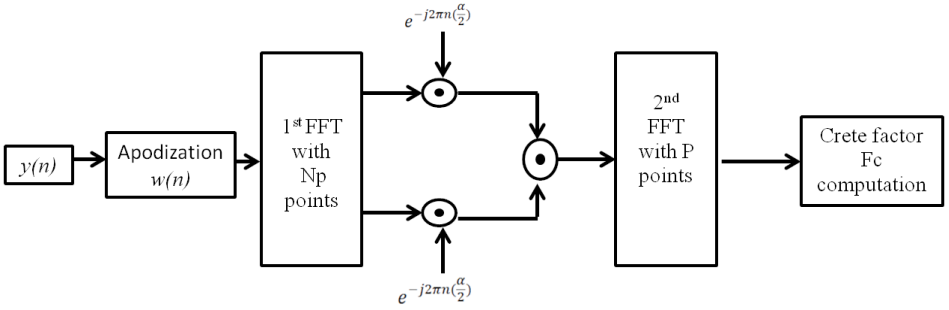

Figure 16. Different steps of the CFD detection process.

The apodization equation is defined as follows:

$$r_k = w_k y_k; \qquad k = 1..N_p \tag{54}$$

where w_k denotes the Hamming window coefficients, y_k is the samples of the observed signal $y(n)$, and r_k becomes the coefficients resulting from the apodization.

The apodization step requires PN_p multiplication operations. The second step in the CFD detection process is the first FFT applied on apodized blocks. The complexity of FFT computation is known as $N_p \log_2 N_p$. Consequently, the P apodized blocks require $PN_p log_2 N_p$ multiplication operations. The complex demodulates computation requires PN_p^2 multiplication operations, and the step of complex demodulates multiplication requires $P^2 N_p^2$ multiplication operations.

The second FFT with P data points to obtain the estimation of cyclic spectrum requires $N_p^2 P \log_2 P$ multiplication operation and the calculation of crest factor F_c alone requires $2N + 1$ multiplication operations.

Finally, the algorithmic complexity of CFD, C_{CFD}, is

$$C_{CFD} = 34N^2 + 64NL + 10N + 2 \tag{55}$$

6.3. Algorithmic Complexity of Recurrence-Analysis-Based Detector

To make decisions, the RAD uses a statistic test defined in Equation (18). The RAD detection process is summarized in Figure 17.

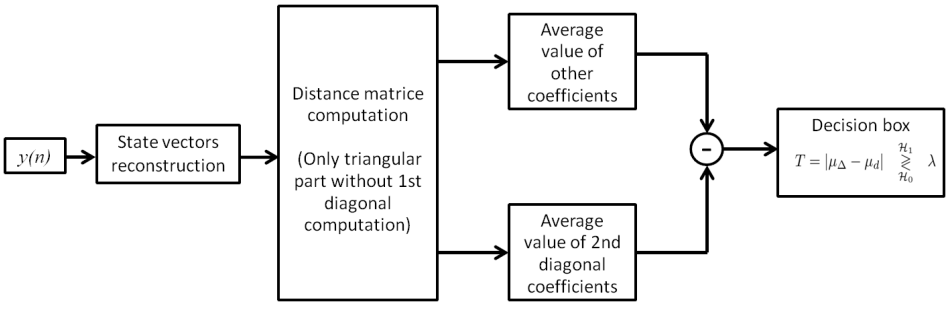

Figure 17. Different steps of the RAD detection process.

The algorithmic complexity of the RAD essentially concerns the distance matrix computation and the calculation of average values of distance matrix coefficients. From the observed signal $y(n)$ containing N samples, we obtain $K = N - (m-1)\tau$ state vectors. Each state vector contains m coordinates. The distance $d_{ij} = \|\mathbf{x}_- \mathbf{x}_j\|$ from the state vector $\mathbf{x}_i$ to other state vectors $\mathbf{x}_j$ requires mK addition operations. Because we exploit only the upper triangular part of the distance matrix with the main diagonal coefficients, we use $\frac{m}{2}K(K-2)$ addition operations. The computation of the average value of the first upper diagonal requires K elementary operations, and the average value of other coefficients

requires $\frac{(K-2)^2}{2}$ elementary operations. The statistic test of the RAD requires one addition operation. Consequently, the computation complexity C_{RAD} of the RAD becomes

$$C_{RAD} = 2N^2 + 4N(\tau - m\tau - 1) + \left[2(m\tau)^2 + 2\tau^2 - 4m\tau^2 - 4\tau + 2m\tau + 6\right] \quad (56)$$

From Equations (52), (55), and (56), in Figure 18, we generated the curves of the evolution of the algorithmic complexity of the ED, CFD, and RAD based on the number of samples contained in the observed signal $y(n)$. The results in Figure 18 show that ED is the simplest algorithm, whereas CFD is the most complicated one. We also notice that the RAD algorithm is less complicated than the CFD algorithm.

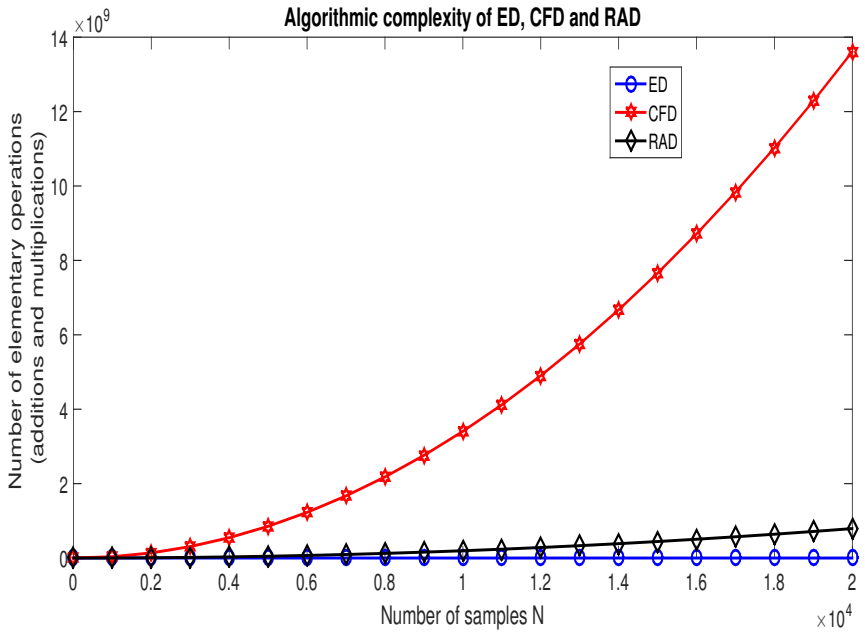

Figure 18. Curves of the algorithmic complexity of ED, CFD, and RAD.

7. Conclusions

This paper deals with the problem of noncooperative spectrum sensing in very low SNR conditions. Many algorithms have recently been developed to overcome the scarcity of radio spectrum. However, most of them suffer from noise uncertainty and do not work correctly in very low SNR conditions. In this paper, we use the promising approach of the Recurrence Quantification Analysis (RQA) to propose a robust detection model, named the Recurrence-Analysis-based Detector (RAD). The RAD benefits from the exploitation of the similitude among the different state vectors. Indeed, our analyses reveal that for a White Gaussian Noise, the coefficients contained on the first upper diagonal are representative of other coefficients of the distance matrix, which is not the case for a communication signal. Thus, by applying a conformity test between the coefficients of the first upper diagonal and other coefficients of the distance matrix, the presence or absence of a communication signal can be revealed. The RAD presents five major advantages: it is more robust than the Energy Detector (ED) and the Cyclostationary Feature Detector (CFD), which are widely used in the noncooperative spectrum sensing context; it does not suffer from noise variance estimation, because the estimation of the noise variance is not required during the spectrum sensing process; it is able to detect the communication signal in a very low SNR condition; contrary to the ED, the RAD is able to distinguish a noisy communication signal and a high energy noise; the RAD does not need a high computational cost like the CFD. Our present work also presents two major contributions. First, we determined, for digital communication signals, the optimal values of the time delay τ and embedding dimension m needed for the phase space reconstruction. Second, we established the analytical expression of detection threshold λ, the probability of detection P_d, and the probability of false alarm P_{fa} of the

detection model based on RQA. From the ROC curves, we can notice without ambiguity that the RAD is more robust than the ED and CFD algorithms. Our current simulations show that the RAD is able to detect the communication signal for SNR ≥ -12 dB. In addition to facilitating the blind detection of communication signals, RQA could be used to accurately estimate the characteristic frequencies of the signal of interest. In our future work, we will optimize the performance of the RAD detector based on this reliable estimation of the characteristic frequencies of the signal of interest.

Author Contributions: Conceptualization, J.-M.K. and A.M.; J.-M.K. developed the proposed approach, performed the principle, and the simulations and prepared the manuscript; K.C.Y. and D.L.J. participated in the development of the theoretical study and reviewed the manuscript. All authors have read and agreed to the published version of the manuscript.

Funding: This research received no external funding.

Data Availability Statement: Dataset available on request from the authors.

Conflicts of Interest: The authors declare no conflict of interest.

References

1. Haykin, S. Cognitive radio: Brain-empowered wireless communications. *IEEE J. Sel. Areas Commun.* **2005**, *23*, 201–220. [CrossRef]
2. Mansour, A.; Mesleh, R.; Abaza, M. New challenges in wireless and free space optical communications. *Opt. Lasers Eng.* **2017**, *89*, 95–108. [CrossRef]
3. Nasser, A.; Mansour, A.; Yao, K.C.; Chaitou, M.; Charara, H. Spatial and time diversities for canonical correlation significance test in spectrum sensing. In Proceedings of the Signal Processing Conference (EUSIPCO), 2016 24th European, Budapest, Hungary, 29 August–2 September 2016; pp. 1232–1236.
4. Nasser, A.; Mansour, A.; Yao, K.C.; Charara, H.; Chaitou, M. Spectrum sensing for full-duplex cognitive radio systems. In Proceedings of the International Conference on Cognitive Radio Oriented Wireless Networks (CROWNCOM), Grenoble, France, 30 May–1 June 2016; Springer: Cham, Switzerland, 2016; pp. 363–374.
5. Nasser, A.; Mansour, A.; Yao, K.; Abdallah, H.; Charara, H. Spectrum sensing based on cumulative power spectral density. *EURASIP J. Adv. Signal Process.* **2017**, *1*, 38–56. [CrossRef]
6. Moawad, A.; Yao, K.; Mansour, A.; Gautier, R. Autocepstrum Approach for Spectrum Sensing in Cognitive Radio. In Proceedings of the 2018 15th International Symposium on Wireless Communication Systems (ISWCS), Lisbon, Portugal, 28–31 August 2018; pp. 1–6.
7. Ding, G.; Wang, J.; Wu, Q.; Zhang, L.; Zou, Y.; Yao, Y.; Chen, Y. Robust Spectrum Sensing With Crowd Sensors. *IEEE Trans. Commun.* **2014**, *62*, 3129–3143. [CrossRef]
8. Luo, L.; Roy, S. Efficient Spectrum Sensing for Cognitive Radio Networks via Joint Optimization of Sensing Threshold and Duration. *IEEE Trans. Commun.* **2012**, *60*, 2851–2860. [CrossRef]
9. Zeng, Y.; Liang, Y. Eigenvalue-based spectrum sensing algorithms for cognitive radio. *IEEE Trans. Commun.* **2009**, *57*, 1784–1793. [CrossRef]
10. Li, B.; Li, S.; Nallanathan, A.; Nan, Y.; Zhao, C.; Zhou, Z. Deep Sensing for Next-Generation Dynamic Spectrum Sharing: More Than Detecting the Occupancy State of Primary Spectrum. *IEEE Trans. Commun.* **2015**, *63*, 2442–2457. [CrossRef]
11. Burel, G.; Bouder, C.; Berder, O. Detection of direct sequence spread spectrum transmissions without prior knowledge. In Proceedings of the GLOBECOM'01, IEEE Global Telecommunications Conference, San Antonio, TX, USA, 25–29 November 2001; Volume 1, pp. 236–239.
12. Zhang, X.; Gao, F.; Chai, R.; Jiang, T. Matched filter based spectrum sensing when primary user has multiple power levels. *China Commun.* **2015**, *12*, 21–31. [CrossRef]
13. Kadjo, J.M.; Yao, K.C.; Mansour, A. Blind detection of cyclostationary features in the context of Cognitive Radio. In Proceedings of the IEEE International Symposium on Signal Processing and Information Technology (ISSPIT), Limassol, Cyprus, 12–14 December 2016; pp. 150–155.
14. Sobron, I.; Diniz, P.S.R.; Martins, W.A.; Velez, M. Energy Detection Technique for Adaptive Spectrum Sensing. *IEEE Trans. Commun.* **2015**, *63*, 617–627. [CrossRef]
15. Lopez-Benitez, M.; Casadevall, F. Signal Uncertainty in Spectrum Sensing for Cognitive Radio. *IEEE Trans. Commun.* **2013**, *61*, 1231–1241. [CrossRef]
16. Yang, K.; Huang, Z.; Wang, X.; Li, X. A Blind Spectrum Sensing Method Based on Deep Learning. *Sensors* **2019**, *19*, 2270. [CrossRef]
17. Xue, H.; Gao, F. A machine learning based spectrum-sensing algorithm using sample covariance matrix. In Proceedings of the 2015 10th International Conference on Communications and Networking in China (ChinaCom), Shanghai, China, 15–17 August 2015; pp. 476–480.

18. Zhang, K.; Li, J.; Gao, F. Machine learning techniques for spectrum sensing when primary user has multiple transmit powers. In Proceedings of the 2014 IEEE International Conference on Communication Systems, Macau, China, 19–21 November 2014; pp. 137–141.
19. Xiao, H.; Zhou, X.; Tian, Y. Research on Wireless Spectrum Sensing Technology Based on Machine Learning. In *Proceedings of the International Conference on Security, Privacy and Anonymity in Computation, Communication and Storage*; Springer: Berlin/Heidelberg, Germany, 2018; pp. 472–479.
20. Kadjo, J.M.; Yao, K.C.; Mansour, A. Blind Spectrum Sensing Based on Recurrence Quantification Analysis in the Context of Cognitive Radio. In Proceedings of the 26th European Signal Processing Conference (EUSIPCO), Rome, Italy, 3–7 September 2018; pp. 1835–1839.
21. Ünal, B. Stability Analysis of Bitcoin using Recurrence Quantification Analysis. *Chaos Theory Appl.* **2022**, *4*, 104–110. [CrossRef]
22. Martín, C.J.; Itayetzin, B.C.V.; Gertrudis, H.G.G.; Claudia, L. Nonlinear Dynamics of Heart Rate Variability after Acutely Induced Myocardial Ischemia by Percutaneous Transluminal Coronary Angioplasty. *Entropy* **2023**, *25*, 469. [CrossRef]
23. Costa, D.G.d.B.; Reis, B.M.d.F.; Zou, Y.; Quiles, M.G.; Macau, E.E. Recurrence density enhanced complex networks for nonlinear time series analysis. *Int. J. Bifurc. Chaos* **2018**, *28*, 1850008. [CrossRef]
24. Zhang, Q.; Chen, X.; Yin, F.; Hong, F. Analysis and Research on Chaotic Dynamics of Evaporation Duct Height Time Series with Multiple Time Scales. *Atmosphere* **2022**, *13*, 2072. [CrossRef]
25. Marwan, N.; Kurths, J. Cross recurrence plots and their applications. In *Mathematical Physics Research at the Cutting Edge*; Nova Science Publishers: Hauppauge, NY, USA, 2004 ; pp. 101–139.
26. Atapattu, S.; Tellambura, C.; Jiang, H. *Energy Detection for Spectrum Sensing in Cognitive Radio*; Springer: New York, NY, USA, 2014.
27. Mitola, J.; Maguire, G.Q. Cognitive radio: Making software radios more personal. *IEEE Pers. Commun.* **1999**, *6*, 13–18. [CrossRef]
28. Mitola, J. Cognitive Radio Architecture Evolution. *Proc. IEEE* **2009**, *97*, 626–641. [CrossRef]
29. Naraghi-Pour, M.; Ikuma, T. Autocorrelation-Based Spectrum Sensing for Cognitive Radios. *IEEE Trans. Veh. Technol.* **2010**, *59*, 718–733. [CrossRef]
30. Marwan, N.; Romano, M.C.; Thiel, M.; Kurths, J. Recurrence plots for the analysis of complex systems. *Phys. Rep.* **2007**, *438*, 237–329. [CrossRef]
31. Webber, C.L., Jr.; Zbilut, J.P. Recurrence quantification analysis of nonlinear dynamical systems. *Tutor. Contemp. Nonlinear Methods Behav. Sci.* **2005**, *94*, 26–94.
32. Anishchenko, V.S.; Astakhov, V.; Neiman, A.; Vadivasova, T.; Schimansky-Geier, L. *Nonlinear Dynamics of Chaotic and Stochastic Systems: Tutorial and Modern Developments*; Springer: Berlin/Heidelberg, Germany, 2007.
33. Williams, G. *Chaos Theory Tamed*; Routledge: London, UK, 2014. [CrossRef]
34. Ivancevic, V.G.; Ivancevic, T.T. *Complex Nonlinearity: Chaos, Phase Transitions, Topology Change and Path Integrals*; Springer: Berlin/Heidelberg, Germany, 2008.
35. Kantz, H.; Schreiber, T. *Nonlinear Time Series Analysis*; Cambridge University Press: Cambridge, UK, 2004; Volume 7.
36. Marwan, C.W.N. Mathematical and Computational Foundations of Recurrence Quantifications. In *Recurrence Quantification Analysis. Understanding Complex Systems*; Springer: Cham, Switzerland; AIP Publishing: Melville, NY, USA, 2015. Available online: https://ouci.dntb.gov.ua/en/works/leGrnZW7/ (accessed on 17 June 2024).
37. Bradley, E.; Kantz, H. Nonlinear time-series analysis revisited. *Chaos Interdiscip. J. Nonlinear Sci.* **2015**, *25*, 097610. [CrossRef]
38. Chelidze, D. Reliable Estimation of Minimum Embedding Dimension Through Statistical Analysis of Nearest Neighbors. *J. Comput. Nonlinear Dyn.* **2017**, *12*, 051024. [CrossRef]
39. Kraskov, A.; Stögbauer, H.; Grassberger, P. Estimating mutual information. *Phys. Rev. E* **2004**, *69*, 066138. [CrossRef]
40. Fraser, A.M.; Swinney, H.L. Independent coordinates for strange attractors from mutual information. *Phys. Rev. A* **1986**, *33*, 1134. [CrossRef]
41. David, C.; Joseph, P.C. *Experimental Nonlinear Dynamics Notes for MCE 567*; Cambridge University Press: New York, NY, USA, 2000.
42. Cao, L. Practical method for determining the minimum embedding dimension of a scalar time series. *Phys. D Nonlinear Phenom.* **1997**, *110*, 43–50. [CrossRef]
43. Kennel, M.B.; Brown, R.; Abarbanel, H.D.I. Determining embedding dimension for phase-space reconstruction using a geometrical construction. *Phys. Rev. A* **1992**, *45*, 3403–3411. [CrossRef]
44. Takens, F. Detecting strange attractors in turbulence. In *Dynamical Systems and Turbulence, Warwick 1980*; Springer: Berlin/Heidelberg, Germany, 1981; pp. 366–381.
45. Webber, C.L., Jr.; Zbilut, J.P. Dynamical assessment of physiological systems and states using recurrence plot strategies. *J. Appl. Physiol.* **1994**, *76*, 965–973. [CrossRef]
46. Zbilut, J.P.; Webber, C.L., Jr. Recurrence quantification analysis: Introduction and historical context. *Int. J. Bifurc. Chaos* **2007**, *17*, 3477–3481. [CrossRef]
47. Thiel, M.; Romano, M.C.; Kurths, J.; Meucci, R.; Allaria, E.; Arecchi, F.T. Influence of observational noise on the recurrence quantification analysis. *Phys. D Nonlinear Phenom.* **2002**, *171*, 138–152. [CrossRef]
48. Mansour, A. *Probabilités et Statistiques pour les Ingénieurs: Cours, Exercices et Programmation*; Hermes Science: Paris, France, 2007.
49. Shorack, G.R.; Wellner, J.A. *Empirical Processes with Applications to Statistics*; SIAM: University City, PA, USA, 2009.
50. Gooch, J.W. *Encyclopedic Dictionary of Polymers*; Springer: New York, NY, USA, 2010.

51. Abell, M.L.; Braselton, J.P.; Rafter, J.A.; Rafter, J.A. *Statistics with Mathematica*; Academic Press: San Diego, CA, USA, 1999.
52. Papoulis, A.; Pillai, S.U. *Probability, Random Variables, and Stochastic Processes*; McGraw-Hill Education: New York, NY, USA, 2002.
53. Miller, S.; Childers, D. *Probability and Random Processes: With Applications to Signal Processing and Communications*; Academic Press: Cambridge, MA, USA, 2012.
54. Kha, Q.H.; Ho, Q.T.; Le, N.Q.K. Identifying SNARE Proteins Using an Alignment-Free Method Based on Multiscan Convolutional Neural Network and PSSM Profiles. *J. Chem. Inf. Model.* **2022**, *62*, 4820–4826. [CrossRef]
55. Nasser, A. Spectrum Sensing for Half and Full-Duplex Interwave Cognitive Radio System. Ph.D. Thesis, Université de Bretagne Occidentale, Brest, France, 2017.
56. Chin, W.L.; Li, J.M.; Chen, H.H. Low-complexity energy detection for spectrum sensing with random arrivals of primary users. *IEEE Trans. Veh. Technol.* **2015**, *65*, 947–952. [CrossRef]
57. Cohen, D.; Eldar, Y.C. Sub-Nyquist cyclostationary detection for cognitive radio. *IEEE Trans. Signal Process.* **2017**, *65*, 3004–3019. [CrossRef]
58. Tani, A.; Fantacci, R.; Marabissi, D. A low-complexity cyclostationary spectrum sensing for interference avoidance in femtocell LTE-A-based networks. *IEEE Trans. Veh. Technol.* **2015**, *65*, 2747–2753. [CrossRef]
59. Ahmadi, S.; Srinivasan, R.M.; Cho, H.; Park, J.; Cho, J.; Park, D. *Channel Models for IEEE 802.16 m Evaluation Methodology Document*; IEEE 802.16 Broadband Wireless Access Working Group: 2007; pp. 3–12. Available online: https://standards.ieee.org/ieee/802.16g/3635/ (accessed on 17 June 2024).
60. Zayen, B.; Guibène, W.; Hayar, A. Performance comparison for low complexity blind sensing techniques in cognitive radio systems. In Proceedings of the 2010 2nd International Workshop on Cognitive Information Processing, Elba Island, Italy, 14–16 June 2010; pp. 328–332. [CrossRef]
61. Gardner, W. *Cyclostationarty in Communications and Signal Processing*; IEEE PRESS: New York, NY, USA, 1994.
62. Gardner, W. The spectral correlation theory of Cyclostationary time-series. *Signal Process.* **1986**, *11*, 13–36. [CrossRef]
63. Gardner, W. Exploitation Of Spectral Redundancy In Cyclostationary Signals. *IEEE Signal Process. Mag.* **1991**, *8*, 14–36. [CrossRef]